Hindawi Publishing Corporation
Mathematical Problems in Engineering
Volume 2009, Article ID 802970, 19 pages
doi:10.1155/2009/802970

Research Article

Chaotic Patterns in Aeroelastic Signals

F. D. Marques and R. M. G. Vasconcellos

Laboratory of Aeroelasticity, School of Engineering of São Carlos, University of São Paulo, Avenue Trabalhador Sancarlense, 400, 13566-590 São Carlos, SP, Brazil

Correspondence should be addressed to F. D. Marques, fmarques@sc.usp.br

Received 1 December 2008; Revised 18 February 2009; Accepted 24 August 2009

Recommended by Elbert E. Neher Macau

This work presents the analysis of nonlinear aeroelastic time series from wing vibrations due to airflow separation during wind tunnel experiments. Surrogate data method is used to justify the application of nonlinear time series analysis to the aeroelastic system, after rejecting the chance for nonstationarity. The singular value decomposition (SVD) approach is used to reconstruct the state space, reducing noise from the aeroelastic time series. Direct analysis of reconstructed trajectories in the state space and the determination of Poincaré sections have been employed to investigate complex dynamics and chaotic patterns. With the reconstructed state spaces, qualitative analyses may be done, and the attractors evolutions with parametric variation are presented. Overall results reveal complex system dynamics associated with highly separated flow effects together with nonlinear coupling between aeroelastic modes. Bifurcations to the nonlinear aeroelastic system are observed for two investigations, that is, considering oscillations-induced aeroelastic evolutions with varying freestream speed, and aeroelastic evolutions at constant freestream speed and varying oscillations. Finally, Lyapunov exponent calculation is proceeded in order to infer on chaotic behavior. Poincaré mappings also suggest bifurcations and chaos, reinforced by the attainment of maximum positive Lyapunov exponents.

1. Introduction

The assessment of aeroelastic phenomena with linear models has provided a reasonable amount of tools for the analysis of most of adverse instability behavior [1, 2]. Nonetheless, aeronautical engineering has shown advances that lead to faster and lighter aircraft, thereby increasing the risk of moderate or severe nonlinear aeroelastic problems.

Nonlinear behavior is inherent to aeroelastic systems and can be associated with aerodynamic sources (compressibility, separated flows, aerodynamic heating, and turbulence effects) and structural sources (effects of aging, loose attachments, material features, and large deformations) [3–5]. Aeroelastic systems can face those effects, for instance, in transonic flight, high angle of attack manoeuvres, and in all cases leading to complex models beyond linearity suppositions. Nonlinear systems typically present features like,

multiple equilibrium points, bifurcations, limit-cycle oscillations, and chaos [6, 7]. The presence of such effects results in modifications to the aeroelastic dynamics, leading to more laborious prediction of instabilities. For instance, the flutter phenomenon in the presence of nonlinearities happens in a different way to that foreseen in linear models.

Recently, nonlinear aeroelasticity research has been performed for a greater number of groups using advanced CFD methods, reduced-order models, and other methodologies [8–10]. However, these methodologies present deficiencies such as losses in the analysis of the physical phenomenon and little flexibility to evaluate different flight regimes using the same model. To validate and verify the mathematical models, experimental analysis makes it possible to observe the system dynamics without neglecting important effects. Experimental data furnishes sequences of measurements that correspond to time series with embedded system dynamics. Time series analysis techniques, such as state space reconstruction and Lyapunov exponents, can be used in these time series to access important information in the system dynamics. Therefore, it seems reasonable that by examining raw experimental data with techniques from time series analysis, one can better assess the effects of aerodynamic and/or structural nonlinearities on aeroelastic systems. Moreover, such insight may provide important tools to support and improve mathematical modeling for aeroelastic analysis. Nonlinear time series analysis techniques can also have an important impact in flutter flight tests, helping in the extraction of instability parameters which are typically surrounded by uncertainties.

While many processes in nature seem a priori very unlikely to be linear, their possible nonlinear nature might not be evident in specific aspects of their dynamics. Moreover, there is always the danger that one is dealing with nonstationary time series, particularly in the case of experiments. Testing the properties of a time series is the most prudent action before starting to draw any conclusion on a system behavior. A variety of techniques to check time series stationarity are available [11], and the method of surrogate data can also be used to justify the application of nonlinear time series analysis techniques excluding the linear hypothesis [12, 13].

Typical dynamic system responses can be assessed by means of reconstructing the state space from time series using the so-called method of *singular value decomposition* (SVD) [14]. The SVD method uses the properties of the covariance matrix to produce uncorrelated coordinates; as a result of the process the data is filtered, diminishing complications caused by the noise present in experimental data.

With reconstructed state spaces and Poincaré sections, it is possible to identify structures associated with limit-cycle oscillations (LCOs) and chaotic patterns [15, 16]. Chaotic behavior may be characterized by the divergence between neighbor trajectories in state space [17]. The assessment of Lyapunov exponents can be used to quantify this divergence [15].

The purpose of this work is to apply techniques from time series analysis for the investigation of nonlinear aeroelastic response behavior present in experimental data obtained from a wind tunnel tests. The experimental apparatus comprises a flexible wing model and by exposing it to the wind tunnel airflow, motion-induced aeroelastic responses occur. By inducing motions at higher angles of attack, flow separation introduces severe unsteady aerodynamic nonlinearity into the system. Incidence oscillatory variations are achieved using a turntable that supports the wing model, and structural deformations are captured by strain gages, thereby providing information on the aeroelastic responses. In this way, investigations may be made for various wind tunnel freestream speed and turntable oscillation frequencies.

The resulting aeroelastic signals are firstly checked for stationarity and nonlinearity properties. Runtest and reverse arrangements followed by surrogate data tests are used to the aforementioned time series properties checking.

The SVD method is used to reconstruct the state space from aeroelastic time series. Evolutions of reconstructed state space and respective Poincaré mapping with parameter variation are presented and discussed. Finally, the method for estimating the largest Lyapunov exponents is applied to identify and reinforce the suspect for the presence of deterministic chaotic behavior in the aeroelastic response time series.

2. State Space Reconstruction

State space reconstruction approaches use time histories or time series ($\mathbf{s}(t)$) to extract the dynamics of a system. Reconstruction techniques are based on Taken's embedded theorem [18], which establishes that a time series $\mathbf{s}(t)$ has information on nonobservable states. With $\mathbf{s}(t)$ it is possible to reconstruct the state space of the system comparable to the real case preserving the invariants of the system, for example, attractor dimension and Lyapunov exponents. This statement has been proven numerically by Packard et al. [19] and Takens [18].

There are different methods to reconstruct the state space, like the *method of delays* (MODs) and the *singular value decomposition method* (SVD). The MOD is the most explored reconstruction method in literature. In this technique a time delay (τ) and an embedding dimension (d) are required to generate delayed coordinates from time series [20].

The reconstruction method based on singular value decomposition (SVD) has been proposed by Broomhead and King [14]. The methodology eliminates the need for a time delay parameter by using the properties of the covariance matrix of the data to generate uncorrelated coordinates. One of the advantages of SVD is the capacity of filtering the time series as a result of the reconstruction process. Kugiumtzis and Christophersen [21] and Vasconcellos [16] have compared MOD and SVD, and they concluded that SVD is more reliable for noisy data, since MOD may lead to arbitrary conclusions because the approaches to obtain τ and d are sensitive to noise [16, 22]. Therefore in principle, the SVD approach is more suitable for experimentally acquired time series.

The SVD approach for state space reconstruction needs the covariance matrix constructed from data contained in the time series $\mathbf{s}(t)$. In this case, each state of the system can be considered a statistical variable, and the diagonalization of covariance matrix separates the states by their variance, allowing the assessment of the system dynamics from those states that have higher variance. As small variance states are dominated by noise, reconstruction is basically attained with filtering. The application of an n-size window to a time series of N_T data points results in a sequence of $N = N_T - (n - 1)$ vectors in the embedding space, that is, $\{\mathbf{x}_i \in \Re^n \mid i = 1, 2, \ldots, N\}$. Such a sequence can be used to construct a so-called trajectory matrix ($\mathbf{X}$), which contains the complete record of patterns that have occurred within the window, that is:

$$\mathbf{X} = \left[\mathbf{x}_1^{\mathrm{T}} \;\; \mathbf{x}_2^{\mathrm{T}} \;\; \cdots \;\; \mathbf{x}_N^{\mathrm{T}}\right]. \tag{2.1}$$

The columns of trajectory matrix constitute the state vectors $\mathbf{x}_i$ on the reconstructed trajectory in embedding space. The N state vectors in embedding space are used, in order to find a set of linearly independent vectors in $\Re^n$, which describe efficiently the attracting

manifold in state space [23]. The $\mathbf{X}$ matrix can be decomposed according to the following relation:

$$\mathbf{X} = \mathbf{SDC}^{\mathrm{T}}, \tag{2.2}$$

where $\mathbf{S} = [\mathbf{s}_1 \ \mathbf{s}_2 \ \cdots \ \mathbf{s}_n]$ and $\mathbf{C} = [\mathbf{c}_1 \ \mathbf{c}_2 \ \cdots \ \mathbf{c}_n]$ are matrices of the respective singular vectors, and $\mathbf{D} = \mathrm{diag}[\sigma_1, \sigma_2, \ldots, \sigma_n]$ is a diagonal matrix of the singular values [14].

The number of independent eigenvectors $\mathbf{c}_i$, which are relevant for the description of the system dynamics, is equal to the number of nonzero eigenvalues σ_i, and they also are the new basis for the trajectories projection. The trajectory can be described in the new basis by projecting the trajectory matrix on the basis by the $\mathbf{XC}$ product, where $\mathbf{C} = \{\mathbf{c}_i, i = 1, \ldots, \mathrm{rank}(\mathbf{XX}^{\mathrm{T}})\}$. The new trajectory matrix $\mathbf{XC}$ is described by the relation:

$$(\mathbf{XC})^{\mathrm{T}}(\mathbf{XC}) = \mathbf{D}^2. \tag{2.3}$$

The relationship given by (2.3) corresponds to the diagonalization of the new covariance matrix, so that in the basis $\mathbf{c}_i$ the components of trajectory are uncorrelated.

When the system is perturbed by external noise the trajectory begins to be diffuse in directions corresponding to zero eigenvalues, where the external perturbation dominates. The projection of trajectory matrix in the basis $\mathbf{C}$ works as a lowpass filter for the entire trajectory. Moreover, the SVD method permits the reconstruction of the original trajectory excluding all dimensions dominated by noise and the retrieval of a filtered time series. The presence of a nonzero constant background, or noise floor, in the spectrum σ_i is sufficient to distinguish the deterministic components [14]. The original trajectory may be reconstructed by

$$\mathbf{X}_d = \sum_{\sigma > \text{noise}} \{\mathbf{X}\mathbf{c}_i\}\mathbf{c}_i^{\mathrm{T}}, \tag{2.4}$$

where σ_i corresponds to a singular value above the noise floor.

3. Tools to Characterize Chaotic Patterns

This section presents some techniques that can be employed for the characterization of complex nonlinear dynamics. There is suggested, as first steps toward chaotic patterns assessment, tests for stationarity and the surrogate data test to the experimental time series. If a time series originates from a unknown process, it is important to investigate if the system parameters remain constant or not during the experiment and whether the data does or not some nonlinear deterministic dependencies [24].

Violations of the fact that the dynamical properties of the system underlying a signal must not change during the observation period can be checked simply by measuring them for several segments of the data set [13]. To investigate if the signal contains some nonlinear deterministic dependencies, a surrogate data test can be useful. The basic idea with respect to the surrogate data technique is to make some hypotheses about the data and then try to contradict this hypothesis. A widely used hypothesis is that colored noise data is generated by a linear stochastic process. Therefore, the data is modified in such a way that the

complete structure, except for the assumed properties, will be destroyed. This may be done by Fourier transforming the data, and by randomly shuffling the phases, the power spectrum or equivalently the autocorrelation function is not affected. A new time series with the same power spectrum is obtained by transforming back into the time domain.

If the original data is just colored noise, estimators of dimension, average mutual information, Lyapunov exponents, prediction errors, and so forth should give the same results for the original time series and the surrogates. If however, the analysis yields significant differences, the original data is more than "just noise" [24].

To improve the statistical robustness, several surrogates are generated. Furthermore, it is necessary to take into account a possibly static nonlinear transformation of the data that would distort the Gaussian distribution of the assumed colored noise as done by Theiler et al. [25].

A powerful tool for the verification of complex dynamics, in particular, to identify chaotic patterns is Poincaré mapping. The Poincaré section of the state space dynamics simplifies the geometric description of the dynamics by removing one of the state space dimensions. For instance, a three-dimensional state space presents the Poincaré section as a two-dimensional plane chosen in such way that the trajectories intersect it transversely.

The key point is that this simplified geometry contains the essential information about the periodicity, quasiperiodicity, chaosity, and bifurcations of the system dynamics [17]. Bifurcation, in this case, is the term used to describe any sudden change in the dynamics of the system due to the respective parametric change. Therefore, for any change on the attractor geometry with a parameter variation, bifurcations can be visualized by plotting one Poincaré section for each parameter value. The Poincaré section computation has been based on Merkwirth et al. [26] and Kantz and Shreiber [13], which proposes the section extracted directly from an embedded time series. The result is a set of $(n-1)$-dimensional vector points, used to perform an orthogonal projection.

Lyapunov exponents determination furnishes important indications with respect to chaotic patterns of dynamic systems. Lyapunov exponents describe the mean exponential increase or decrease of small perturbations on an attractor and are invariant with respect to diffeomorphic changes of the coordinate system [24]. When the largest Lyapunov exponent is positive, the system is said to be chaotic. Direct methods to quantify the largest Lyapunov exponent estimate the divergent motion from the reconstructed space state, without fitting a model to the data.

The method proposed by Sato et al. [27] considers the average exponential growth of the distance of neighboring orbits on a logarithmic scale via prediction error on the number of time steps k, that is:

$$p(k) = \frac{1}{Nt_s}\sum_{n=1}^{N}\log_2\left(\frac{\left\|\mathbf{y}^{n+k} - \mathbf{y}^{nn+k}\right\|}{\left\|\mathbf{y}^{n} - \mathbf{y}^{nn}\right\|}\right), \tag{3.1}$$

where N is the number of data points, t_s is the sampling period, and $\mathbf{y}^{nn}$ is the nearest neighbor of $\mathbf{y}^n$.

The dependence of the prediction error $p(k)$ on the number of time steps k may be divided into three phases: the transient, corresponding to the first phase, where the neighboring orbit converges to the direction corresponding to the largest Lyapunov exponent; the second phase, where the distance grows exponentially with $e^{(\lambda_1 t_s k)}$ until it exceeds the range of validity of the linear approximation of the flow around the reference orbit $\mathbf{y}^{n+k}$;

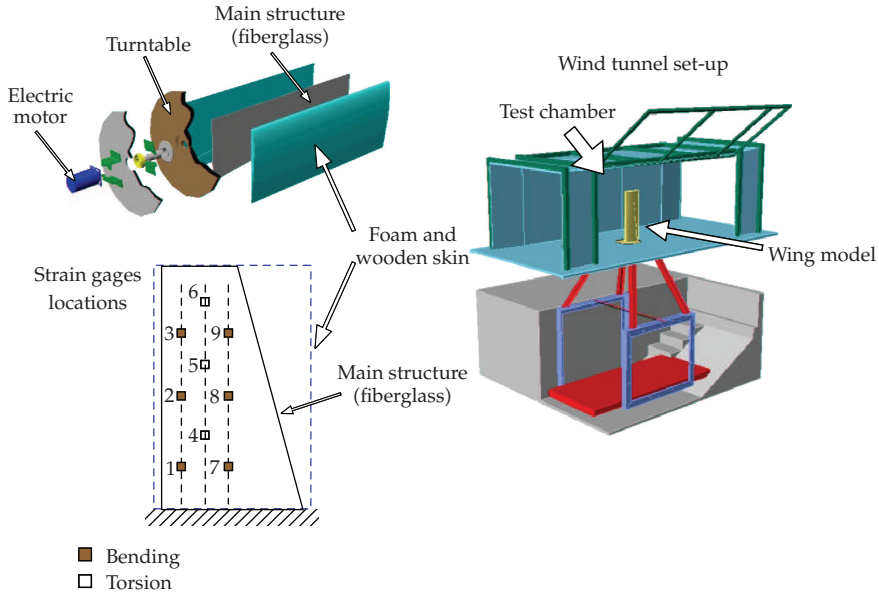

Figure 1: Experimental set-up and strain gages locations.

then, the last phase begins, where the distance increases slower than exponentially until it decreases again due to foldings in the state space [24]. If the second phase is sufficient long, a linear segment with slope λ appears in $p(k)$ versus k plot. This slope value (λ) is associated with the Lyapunov exponent value. This also provides a direct verification of the exponential growth of distances to distinguish deterministic chaos from stochastic processes, where a *non*exponential separation of trajectories occurs [24].

4. Experimental Apparatus and Database

The experimental apparatus comprises an aeroelastic wing model mounted over a turntable device driven by a brushless electrical motor and an acquisition system. The wing model is tested in a wind tunnel test section of approximately 2 m^2 cross-section area and a maximum flow speed of 50 m/s. The wing model was fixed to a turntable that allowed various angles of incidence of the model, thereby providing exploration of a variety of motion-induced aeroelastic responses over a range of airflow velocities.

The wing model main structure was constructed with fiberglass and epoxy resin with a taper ratio of 1 : 1.67, where the width at the root is 250 mm and the semispan is 800 mm. To provide aerodynamic shape of NACA0012 airfoil, high-density foam and a thick wooden skin were used, and the chord was fixed in 290 mm from root to the tip. In order to reduce the effect of aerodynamic cover to the wing structure stiffness, both foam and wooden shell have been segmented at each 100 mm spanwise. Strain gages were fixed to the plate surface to register the dynamic response of the wing main structure. The strain gages were distributed along three spanwise lines. The first and the last lines received three strain gages each, to register bending motions. The intermediate line also received three strain gages, arranged in this case to register torsional motion. Figure 1 illustrates the experimental apparatus with indications of the strain gage locations on the wing model structure.

Table 1: Experimental test cases.

Fixed oscillatory frequency (at 10.0 rad/s)	Fixed freestream speed (at 15.0 m/s)
Freestream speeds (m/s)	Turntable oscillatory frequency (rad/s)
8.28	2.0
9.97	4.0
11.64	6.0
13.30	8.0
14.97	10.0

Data acquisition and motion control of the brushless electrical motor were achieved using a dSPACE DS1103 PPC controller board and real-time interface for SIMULINK. An HBM KWS 3073 amplifier was used to acquire and amplify the strain gages signal. The resulting signals are acquired by the dSPACE controller board, for subsequent storage into a PC compatible computer.

5. Results and Discussion

During experiments, oscillatory motions of the turntable were executed at relatively low amplitude, that is, 5.5° incidence angle, but such oscillations have been considered around an average incidence angle of 9.5°. For these cases, highly unsteady separated flow occurs, inducing complex aeroelastic responses to the wing model. These cases furnish an adequate database for nonlinear aeroelastic response phenomena analysis.

The cases under consideration are summarized in Table 1 and were collected from strain gage at position 1 for bending measurement (cf. Figure 1). Table 1 indicates that aeroelastic time series has been acquired for a range of freestream speed (U), at a fixed turntable oscillatory frequency (ω), and for a range of turntable oscillatory frequencies at a fixed airflow velocity. Both cases provide essential information on motion-induced aeroelastic responses. Each aeroelastic time series has been filtered by SVD method and checked for stationarity with runtest and reverse arrangements test [11], prior to any analysis. All time series considered in this work have passed at the significance level of 0.05. Figure 2 presents a typical aeroelastic response, in this case for $U = 14.97\,\text{m/s}$ and $\omega = 10.0\,\text{rad/s}$, where the existence of complex aeroelastic response can be observed.

In order to justify the use of nonlinear analysis techniques, a surrogate data test was performed. Using Algorithm II of Theiler et al. [25], 99 surrogates were generated and the correlation sum was computed for each by using the algorithm proposed by Grassberger and Procaccia [28]. The correlation sum assesses the relative number of neighboring points closer than r [24] and is given by

$$C_d(r) = \frac{2}{(N-c)(N-1-c)} \sum_{i=1}^{N} \sum_{j=1}^{i-c} H\left(r - \left\|\mathbf{y}^i - \mathbf{y}^j\right\|\right), \tag{5.1}$$

where N is the number of data points, H is the Heaviside function with $H(x) = 1$ for $x > 1$ and zero elsewhere, c is a constant accounting for some correlation length (used to omit points that are close neighbors in time), $\|\mathbf{y}^i - \mathbf{y}^j\|$ is the mutual distance between the points in question, and d is the embedding dimension.

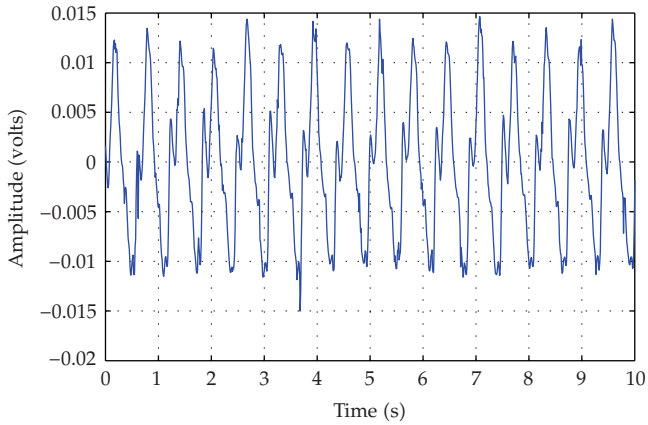

Figure 2: Aeroelastic time series—strain gage measurement at position 1 ($U = 14.97\,\text{m/s}$, $\omega = 10.0\,\text{rad/s}$).

Figures 3 and 4 present the correlation sum of these 99 surrogates in the mean line with the error bars; the correlation sum computed for the SVD-filtered acquired data is present in the continuous line. Clearly, the data is out of correlation sum distribution generated for purely linear stochastic surrogate signal. This evidence reinforces that the signal may be representative of a deterministic nonlinear process. These results provide enough information to qualify further investigation using nonlinear analysis tools to characterize possible aeroelastic chaotic patterns.

Here, state spaces have been reconstructed by the SVD approach. As an example, Figure 5 shows the singular spectrum and the accumulated variance of the considered singular values for one case ($U = 14.97\,\text{m/s}$, $\omega = 10.0\,\text{rad/s}$, and strain gage at position 1—cf. Figure 1), clearly revealing three eigenvalues above the noise floor. This indicates embedding dimension 3, which was confirmed as the same for all the other cases. The state space was reconstructed considering only these tree singular values, which represents more than 99% of the total variance. Figure 6 presents an example of reconstructed state space in terms of the projections onto the three mutually orthogonal planes spanned by the singular vectors ($\mathbf{c}_1, \mathbf{c}_2, \mathbf{c}_3$) and the three-dimensional view. The reconstructed trajectories present complex shapes, with the presence of more than one center of rotation, which is an indication of a chaotic pattern [29].

For the cases presented in Table 1 where a fixed oscillation frequency is considered (in this case, $\omega = 10.0\,\text{rad/s}$) for a range of airflow velocities, respective aeroelastic responses have been used to reconstruct the spaces via the SVD technique. The results furnish an evolution of the reconstructions with respect to freestream speed, allowing investigations of bifurcations and chaotic patterns. Figure 7 shows the evolution of trajectories in reconstructed state space due to freestream speed variation. The occurrence of bifurcation is clear, mainly due to the transition between trajectories at 11.64 and 13.30 m/s as well as between 13.30 and 14.97 m/s. In previous works, Vasconcellos [16] and Marques et al. [30] encountered evidence that bifurcations occur in a similar system. For increasing freestream speed, separated flow intensity also increases and different nonlinear mechanisms for this effect occur.

Poincaré sections of reconstructed state spaces have been determined, in order to supply an easier visualization of the aforementioned transitions or bifurcations. In Figure 8 one may observe considerable changes in the Poincaré sections, as the speed increases, with

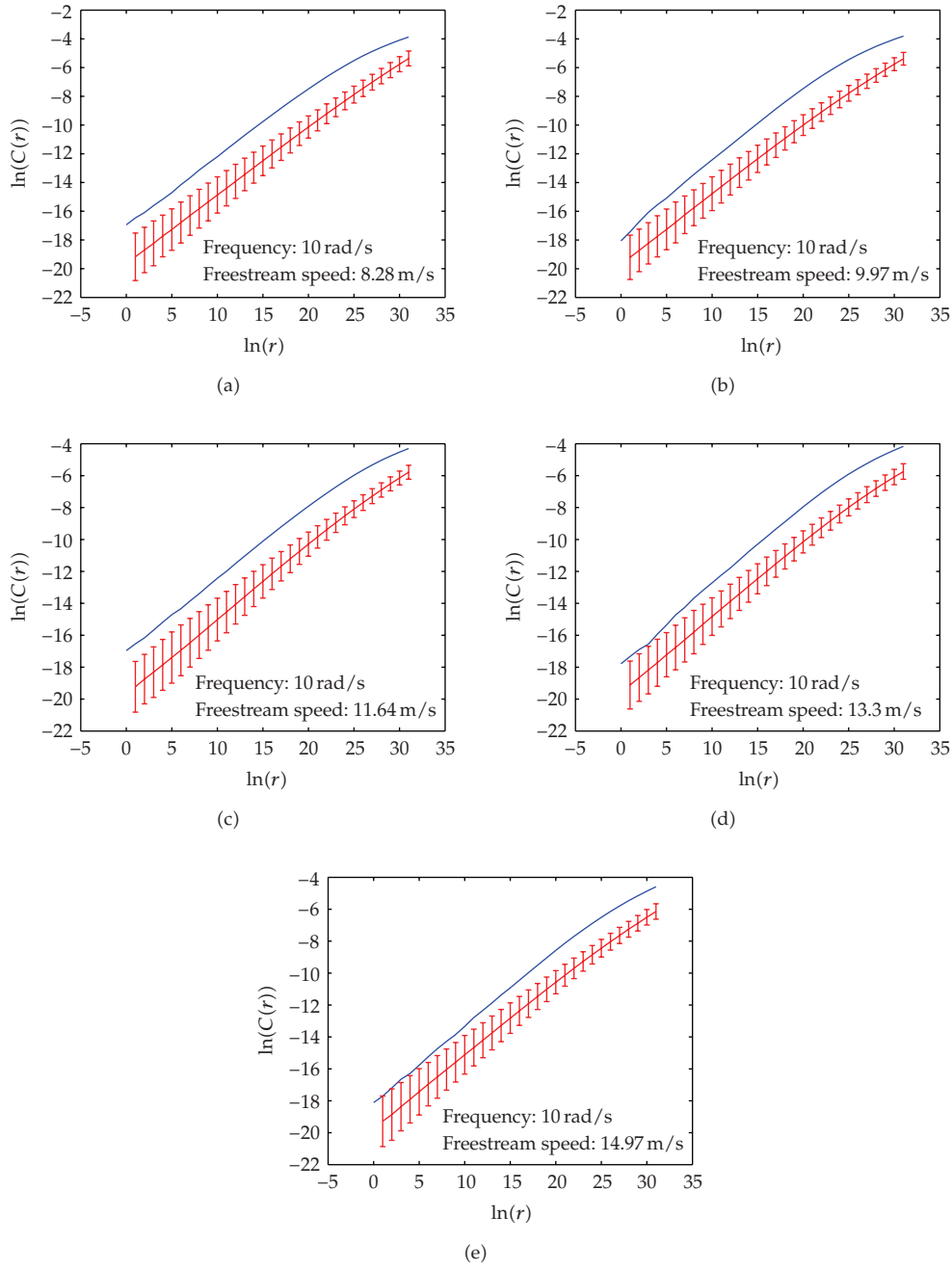

Figure 3: Correlation sum of 99 surrogates (line with error bars) and the tested data for the fixed oscillation frequency conditions.

the amplitude of the motions enlarging. Between third and fourth sections (corresponding to freestream speeds of 11.64 and 13.30 m/s), considerable change in the Poincaré section shape can be observed. The same complex behavior occurs between the fourth and fifth sections (corresponding to freestream speeds of 13.30 and 14.97 m/s). In all these cases, one can infer

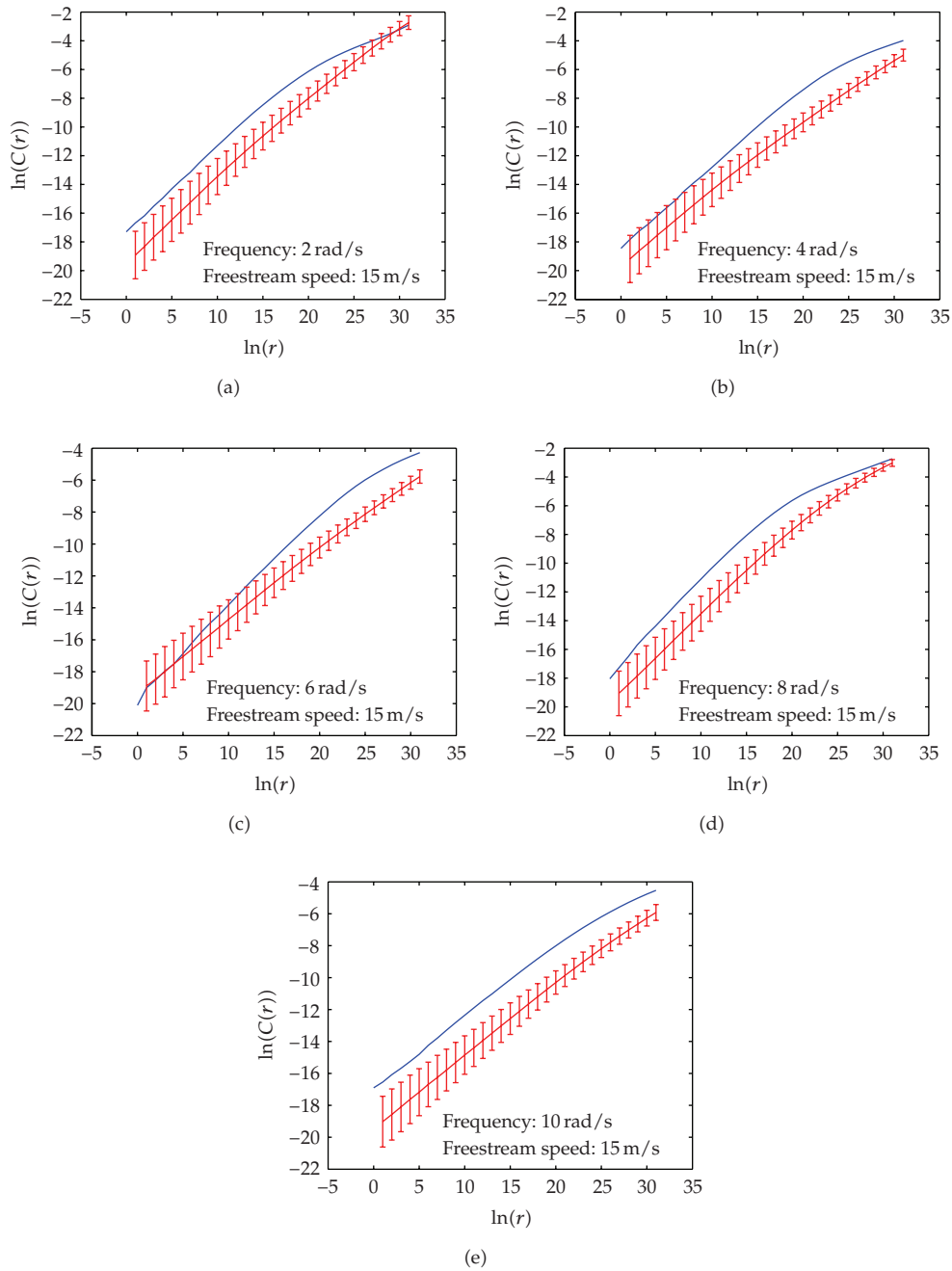

Figure 4: Correlation sum of 99 surrogates (line with error bars) and the tested data for the fixed freestream speed conditions.

that the aeroelastic system response is complex, revealing bifurcations associated separated flowfield effects as well as with distributed structural nonlinearities. Projected Poincaré sections, as illustrated in Figure 9, show an alternative way to visualize the bifurcations with respect to airflow velocity evolution.

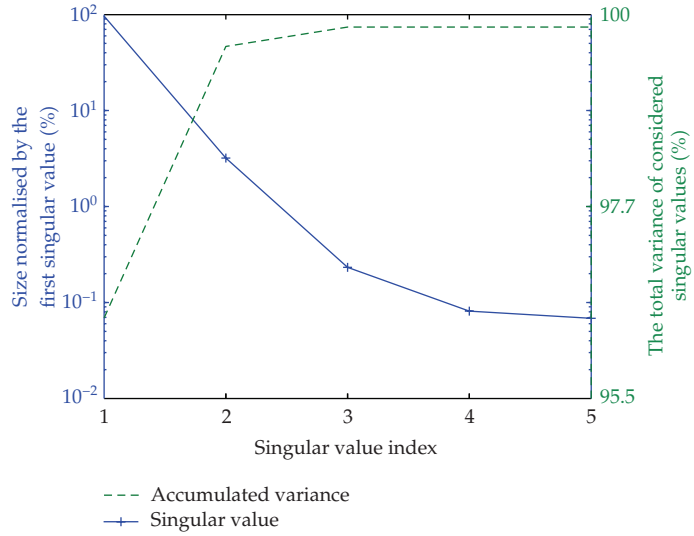

Figure 5: Singular spectrum and accumulated variance for aeroelastic time series (case: $U = 14.97\,\mathrm{m/s}$, $\omega = 10.0\,\mathrm{rad/s}$, and strain gage at position 1—cf. Figure 1).

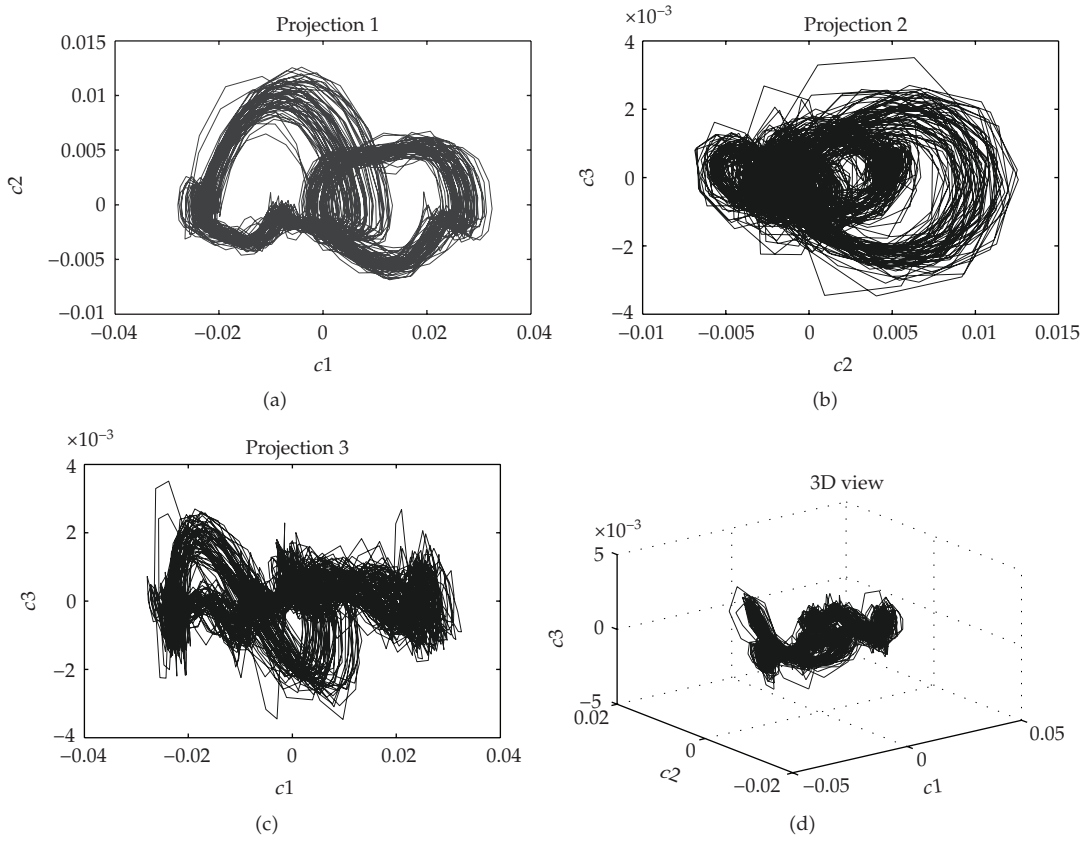

Figure 6: Reconstructed state space for aeroelastic response (case: $U = 14.97\,\mathrm{m/s}$, $\omega = 10.0\,\mathrm{rad/s}$, and strain gage at position 1—cf. Figure 1), including projections in three orthogonal planes and 3D view.

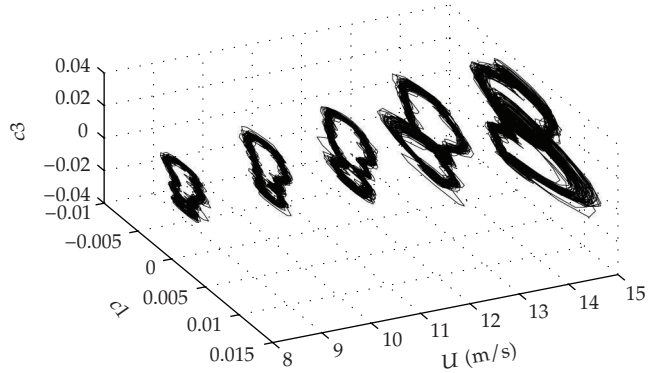

Figure 7: The evolution of state space reconstructions for the case of freestream speed variation: 8.28, 9.97, 11.64, 13.30, and 14.97 m/s, respectively, at fixed oscillatory turntable frequency of $\omega = 10.0$ rad/s.

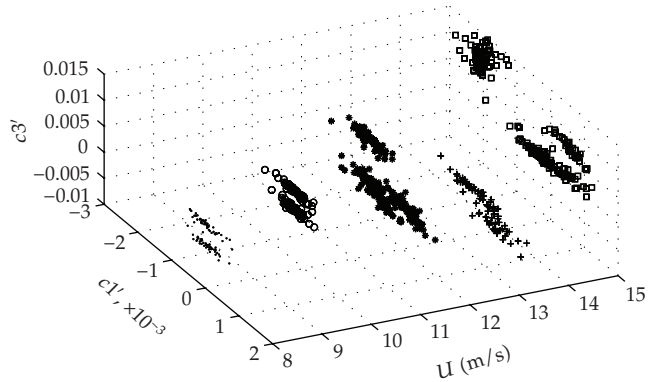

Figure 8: The evolution of Poincaré sections for the case of freestream speed variation: 8.28, 9.97, 11.64, 13.30, and 14.97 m/s, respectively, at fixed oscillatory turntable frequency of $\omega = 10.0$ rad/s.

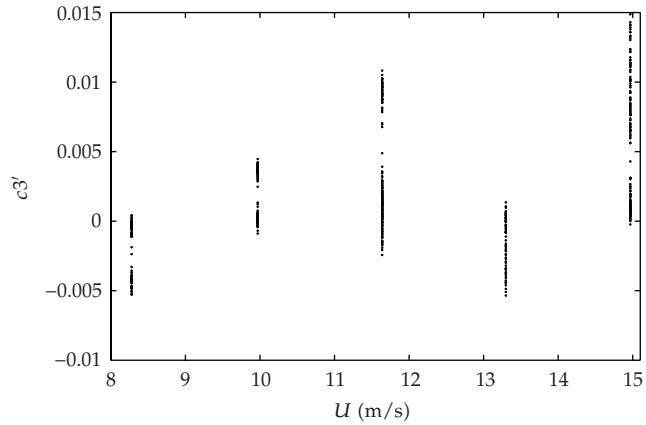

Figure 9: Projection of the Poincaré sections evolution with the freestream speeds: 8.28, 9.97, 11.64, 13.30, and 14.97 m/s, respectively, at fixed oscillatory turntable frequency of $\omega = 10.0$ rad/s.

Table 2: Lyapunov exponents by prediction error technique [27] for fixed turntable oscillatory frequency ($\omega = 10.0\,\text{rad/s}$) and a range of freestream speeds (cf. Table 1).

Freestream speed (m/s)	8.28	9.97	11.64	13.30	14.97
Largest exponent	0.50	0.54	0.56	0.56	0.57

The final step in the investigation of the complex nonlinear behavior of the aeroelastic signals is the determination of the largest Lyapunov exponent. Here, the exponent for each of the aeroelastic responses, for fixed turntable oscillatory frequency in a range of airflow velocities (cf. Table 1), is summarized in Table 2. The calculations were executed using the prediction error technique as proposed by Sato et al. [27]. It may be observed that the largest Lyapunov exponent increases with freestream speed. In all conditions, the largest Lyapunov exponents are positive, indicating chaotic behavior, what implies that the encountered bifurcations from inspecting state space reconstructions and Poincaré mappings are chaos-chaos bifurcations. The occurrence of chaotic motions may cause degradation of aircraft flight performance, leading to future structural problems due to material fatigue. Moreover, abrupt dynamical behavior changes due to bifurcations may yield severe structural damage or total failure.

Figure 10 can be seen as a complementary result, because it shows plottings of solutions for (3.1). The presence of the linear segment slope ensures deterministic chaos occurence, thereby validating surrogate data tests. In Marques et al. [20] and Simoni [31], the method developed by Wolf et al. [32] has been used to estimate the Lyapunov exponents, considering the analysis for similar motion-induced aeroelastic time series. Positive Lyapunov exponents have also been encountered, with values of approximately 0.3. Comparative results between techniques for the largest Lyapunov exponents for nonlinear aeroelastic responses can be found in Marques et al. [33].

The following results are related to investigations of chaotic patterns of aeroelastic responses for a range of turntable oscillatory frequencies, while the wind tunnel freestream speed is kept fixed (in this case, $U = 15.0\,\text{m/s}$). The respective oscillatory frequency range can be seen in Table 1. The state spaces are reconstructed for all these conditions, and Figure 11 shows the evolution of trajectories in state space within the range of turntable oscillatory frequencies. Here, a considerable change in trajectory patterns may be observed, with a clear increase in the amplitude of motion until 8.0 rad/s, followed by a sudden change in shape and amplitude at around 10.0 rad/s. Such behavior may be associated with the so-called bifurcation crises, in which chaotic attractors and their basin of attraction suddenly disappear or expand; the sudden expansion or contraction of a chaotic attractor is called an *interior crises* [17].

The physical events related to these results indicate that separated flow effects and aeroelastic modes interaction play an important role in the nonlinear behavior. Bifurcation crises phenomenon manifests itself due to highly separated flow nonlinearities together with oscillatory evolution leading to nonlinear couplings between different aeroelastic modes.

Poincaré sections obtained from reconstructed state spaces may also be used to verify the peculiar changes in trajectory shape and amplitude. In Figure 12, one may observe considerable changes in Poincaré sections, as the turntable oscillatory frequencies increase, thereby indicating the existence of bifurcations. Again, in all these cases the Poincaré sections suggest complexity of the aeroelastic system and several changes in geometry of state space occur. Again, projected Poincaré sections as shown in Figure 13 can be used to infer the presence of bifurcations.

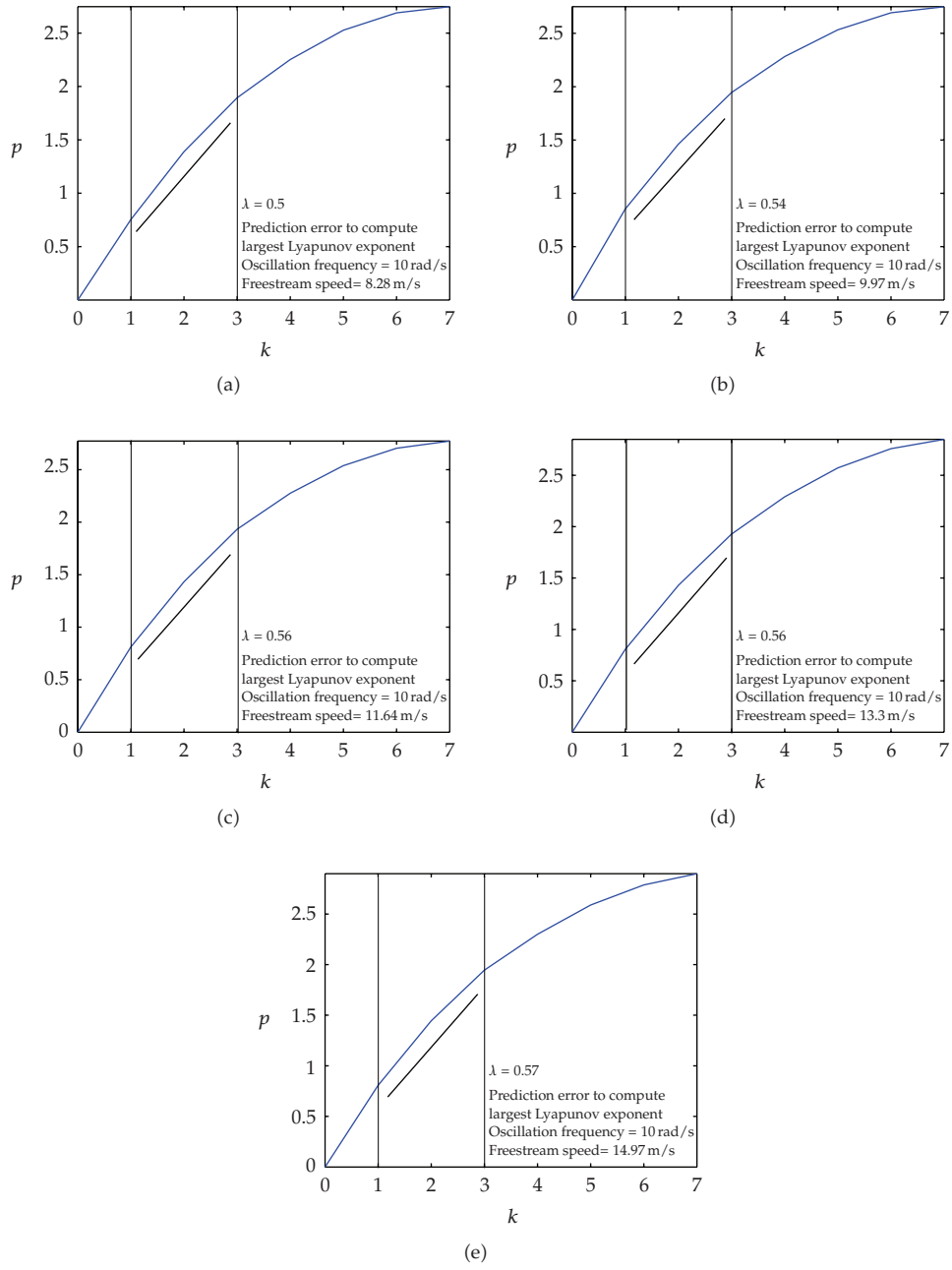

Figure 10: Largest Lyapunov exponents with the freestream speeds: 8.28, 9.97, 11.64, 13.30, and 14.97 m/s, respectively, at fixed oscillatory turntable frequency of $\omega = 10.0$ rad/s.

The largest Lyapunov exponent was also computed via prediction error technique [27], for turntable frequency variation cases (cf. Table 1). In all conditions, the largest Lyapunov exponents are positive as presented in Table 3, indicating chaotic patterns for the aeroelastic wing responses and chaos-chaos bifurcations.

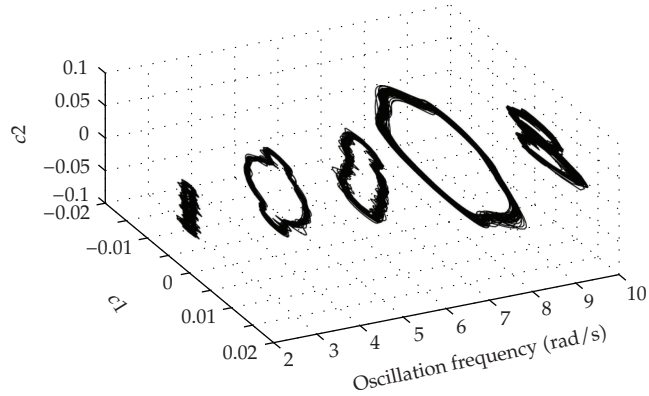

Figure 11: Reconstructed state space evolution with turntable oscillatory frequencies: 2.0, 4.0, 6.0, 8.0, and 10.0 rad/s, respectively, at fixed wind tunnel freestream speed of $U = 15.0\,\mathrm{m/s}$.

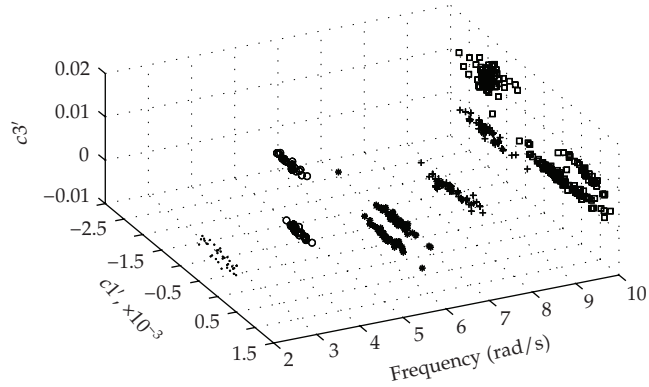

Figure 12: Poincaré sections evolution with turntable oscillatory frequencies: 2.0, 4.0, 6.0, 8.0, and 10.0 rad/s, respectively, at fixed wind tunnel freestream speed of $U = 15.0\,\mathrm{m/s}$.

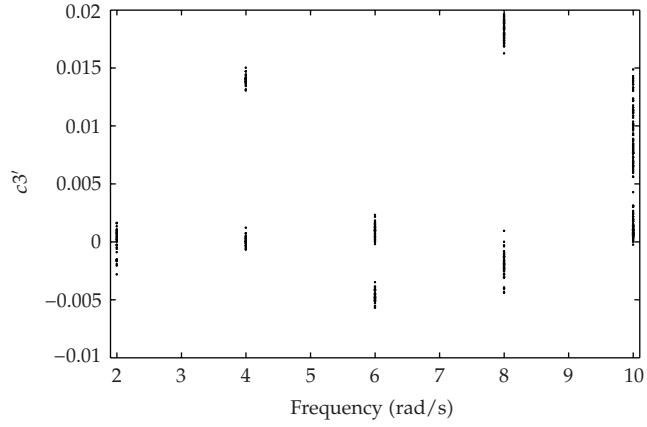

Figure 13: Projection of the Poincaré sections evolution with turntable oscillatory frequencies: 2.0, 4.0, 6.0, 8.0, and 10.0 rad/s, respectively, at fixed wind tunnel freestream speed of $U = 15.0\,\mathrm{m/s}$.

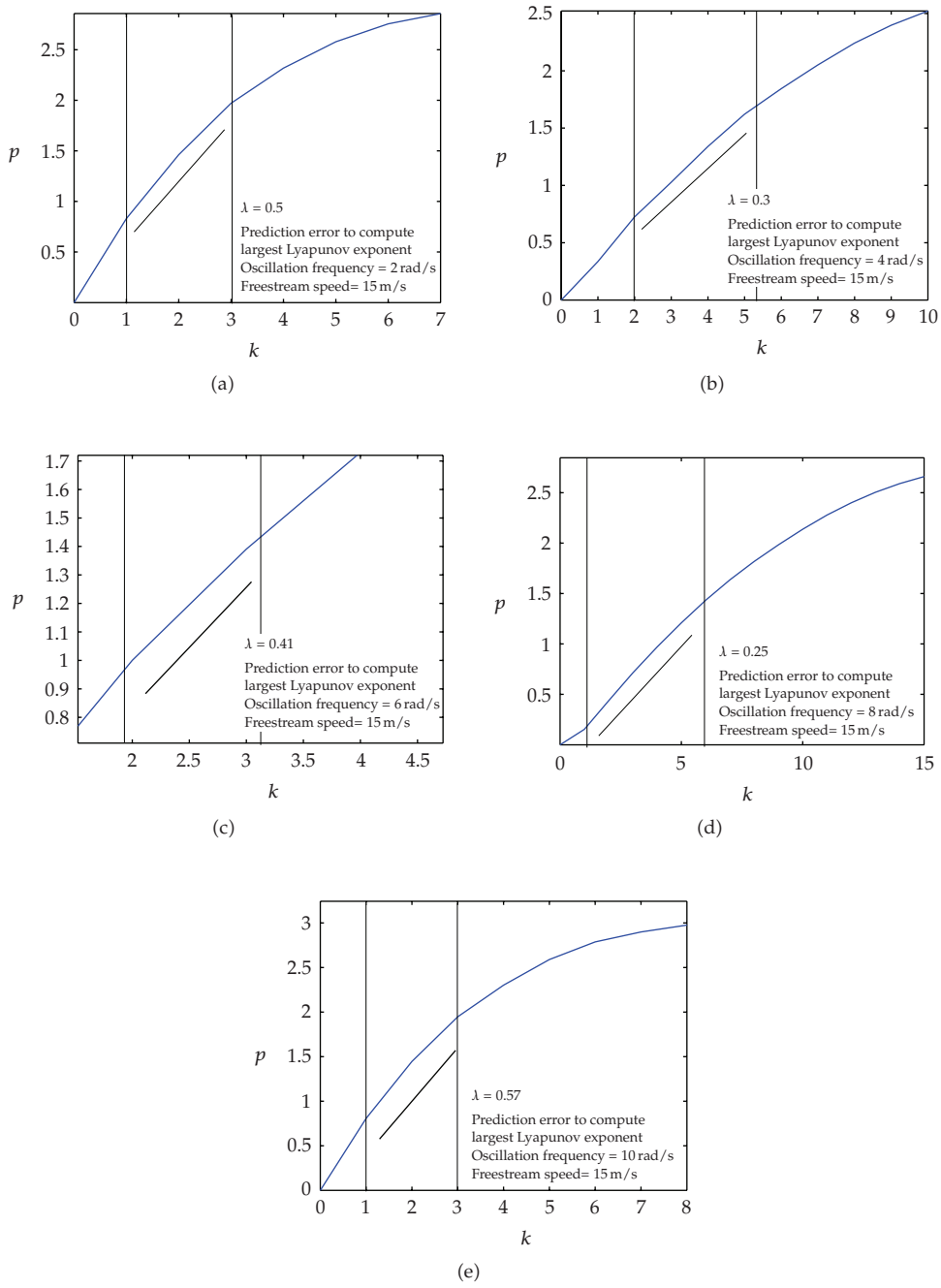

Figure 14: Largest Lyapunov exponents via prediction error computed for turntable oscillatory frequencies: 2.0, 4.0, 6.0, 8.0, and 10.0 rad/s, respectively, at fixed wind tunnel freestream speed of $U = 15.0$ m/s.

Similarly to the previous cases (freestream speed range), Lyapunov exponents for that analysis have been obtained from plottings as presented in Figure 14 and summarized in Table 3.

Table 3: Lyapunov exponents by prediction error technique [27] for fixed wind tunnel freestream speed (U = 15.0 m/s) and a range of turntable oscillatory frequencies (cf. Table 1).

Turntable oscillatory frequency (rad/s)	2.0	4.0	6.0	8.0	10.0
Largest exponent	0.50	0.30	0.41	0.25	0.57

6. Concluding Remarks

Techniques from nonlinear time series analysis theory have been presented in this work to investigate chaotic patterns of nonlinear motion-induced aeroelastic responses. Experimental tests with a wind tunnel aeroelastic wing model mounted on an oscillatory turntable have been executed with highly separated flow field conditions. Aeroelastic time series have been obtained from strain gages measurements, which were used directly with a variety of time series analysis tools. The time series have been tested using the surrogate data method, in order to investigate whether or not the data was representative of a nonlinear process. The results justify the application of techniques in order to search for bifurcations and chaotic patterns, since the linear hypothesis could be rejected.

The SVD method has been used to reconstruct the state spaces from the experimentally acquired aeroelastic time series, and the trajectories and subsequent assessment of the Poincaré sections have indicated complex behavior, such as bifurcations and chaos.

The evolution with freestream speed for a fixed turntable oscillatory frequency suggests the occurrence of chaos-chaos bifurcations, since changes in the shape of the attractor and Poincaré sections have been observed and all largest Lyapunov exponents are positive. Moreover, evolutions in terms of turntable oscillation frequency at a fixed wind tunnel freestream velocity also show the occurrence of bifurcations. Reconstructed spaces have also revealed complex motion amplitude changes with respect to parametric variation (freestream speed or turntable oscillatory frequency).

The occurrence of bifurcations, mainly in the cases where a sudden increase in amplitude of motion happens, reinforces the importance of nonlinear behavior study in aeroelastic systems. Further investigations to check experimental nonlinear aeroelastic response features with other time series analysis tools are planned.

Acknowledgments

The authors acknowledge the financial support of the State of São Paulo Research Agency (FAPESP), Brazil (Grant 2007/08459-1), and the National Council for Scientific and Technological Development (CNPq), Brazil (Grant 306991/2007-1).

References

[1] P. P. Friedmann, "The renaissance of aeroelasticity and its future," in *Proceedings of the International Forum on Aeroelasticity and Structural Dynamics (CEAS '97)*, pp. 19–49, Rome, Italy, June 1997.

[2] I. E. Garrick, "Aeroelasticity—frontiers and beyond," *AIAA Journal of Aircraft*, vol. 13, no. 9, pp. 641–657, 1976.

[3] L. E. Ericsson and J. P. Reding, "Fluid dynamics of unsteady separated flow. Part II. Lifting surfaces," *Progress in Aerospace Sciences*, vol. 24, no. 4, pp. 249–356, 1987.

[4] B. H. K. Lee, S. J. Price, and Y. S. Wong, "Nonlinear aeroelastic analysis of airfoils: bifurcation and chaos," *Progress in Aerospace Sciences*, vol. 35, no. 3, pp. 205–334, 1999.

[5] E. H. Dowell and D. Tang, "Nonlinear aeroelasticity and unsteady aerodynamics," *AIAA Journal of Aircraft*, vol. 40, no. 9, pp. 1697–1707, 2002.
[6] H. Alighanbari and B. H. K. Lee, "Analysis of nonlinear aeroelastic signals," *AIAA Journal of Aircraft*, vol. 40, no. 3, pp. 552–558, 2003.
[7] E. F. Sheta, V. J. Harrand, D. E. Thompson, and T. W. Strganac, "Computational and experimental investigation of limit cycle oscillations of nonlinear aeroelastic systems," *AIAA Journal of Aircraft*, vol. 39, no. 1, pp. 133–141, 2002.
[8] J. W. Edwards, "Computational aeroelasticity," in *Structural Dynamics and Aeroelasticity*, A. K. Noor and S. L. Venner, Eds., vol. 5 of *Flight Vehicle Materials, Structures and Dynamics—Assessment and Future Directions*, pp. 393–436, ASME, New York, NY, USA, 1993.
[9] J. G. Leishman and T. S. Beddoes, "A semi-empirical model for dynamic stall," *Jornal of the American Helicopter Society*, vol. 34, no. 3, pp. 3–17, 1989.
[10] F. D. Marques, *Multi-layer functional approximation of non-linear unsteady aerodynamic response*, Ph.D. thesis, University of Glasgow, Glasgow, UK, 1997.
[11] J. S. Bendat and A. G. Piersol, *Random Data: Analysis & Measurement Procedures*, John Wiley & Sons, New York, NY, USA, 2nd edition, 1986.
[12] T. Schreiber and A. Schmitz, "Surrogate time series," *Physica D*, vol. 142, no. 3-4, pp. 346–382, 2000.
[13] H. Kantz and T. Schreiber, *Nonlinear Time Series Analysis*, Cambridge University Press, Cambridge, UK, 2nd edition, 2004.
[14] D. S. Broomhead and G. P. King, "Extracting qualitative dynamics from experimental data," *Physica D*, vol. 20, no. 2-3, pp. 217–236, 1986.
[15] A. H. Nayfeh and B. Balachandran, *Applied Nonlinear Dynamics*, John Wiley & Sons, New York, NY, USA, 1995.
[16] R. M. G. Vasconcellos, *Reconstrução de espa ços de estados aeroelásticos por decomposiçãao em valores singulares*, M.S. thesis, Universidade de São Paulo—EESC-USP, São Paulo, Brazil, 2007.
[17] R. C. Hilborn, *Chaos and Nonlinear Dynamics: An Introduction for Scientists and Engineers*, The Clarendon Press, Oxford University Press, New York, NY, USA, 2nd edition, 2000.
[18] F. Takens, "Detecting strange attractors in turbulence," in *Dynamical Systems and Turbulence, Lecture Notes in Mathematics*, vol. 898, pp. 366–381, Springer, Berlin, Germany, 1981.
[19] N. J. Packard, J. P. Crutchfield, J. D. Farmer, and R. S. Shaw, "Geometry from a time series," *Physical Review Letters*, vol. 45, no. 9, pp. 712–716, 1980.
[20] F. D. Marques, E. M. Belo, V. A. Oliveira, J. R. Rosolen, and A. R. Simoni, "On the investigation of state space reconstruction of nonlinear aeroelastic response time series," *Shock and Vibration*, vol. 13, no. 4-5, pp. 393–407, 2006.
[21] D. Kugiumtzis and N. Christophersen, "State space reconstruction: method of delays vs singular spectrum approach," Research Report 236, Department of Informatics, University of Oslo, Oslo, Norway, 1997.
[22] M. Casdagli, S. Eubank, D. Farmer, and J. Gibson, "State space reconstruction in the presence of noise," *Physica D*, vol. 51, no. 1–3, pp. 52–98, 1991.
[23] M. A. Athanasiu and G. P. Pavlos, "SVD analysis of the magnetospheric AE index time series and comparison with low-dimensional chaotic dynamics," *Nonlinear Processes in Geophysics*, vol. 8, no. 1-2, pp. 95–125, 2001.
[24] U. ParlitzJ. A. K. Suykens and J. Vandewalle, "Nonlinear time-series analysis," in *Nonlinear Modeling-Advanced Black-Box Techniques*, pp. 209–239, Kluwer Academic Publishers, Boston, Mass, USA, 1998.
[25] J. Theiler, B. Galdrikian, A. Longtin, S. Eubank, and J. D. Farmer, "Using surrogate data to detect nonlinearity in time series," in *Nonlinear Modeling and Forecasting*, vol. 12 of *SFI Studies in the Sciences of Complexity*, pp. 163–188, Addison-Wesley, Reading, Mass, USA, 1992.
[26] C. Merkwirth, U. Parlitz, and W. Lauterborn, "TSTOOL—a software package for nonlinear time series analysis," in *Proceedings of the International Workshop on Advanced Black-Box Techniques for Nonlinear Modeling*, J. A. Suykens and J. Vandewalle, Eds., Katholieke Universiteit Leuven, Leuven, Belgium, July 1998.
[27] S. Sato, M. Sano, and Y. Sawada, "Practical methods of measuring the generalized dimension and the largest Lyapunov exponent in high-dimensional chaotic systems," *Progress of Theoretical Physics*, vol. 77, no. 1, pp. 1–5, 1987.
[28] P. Grassberger and I. Procaccia, "Measuring the strangeness of strange attractors," *Physica D*, vol. 9, no. 1-2, pp. 189–208, 1983.
[29] T. Yalçinkaya and Y.-C. Lai, "Phase characterization of chaos," *Physical Review Letters*, vol. 79, no. 20, pp. 3885–3888, 1997.

[30] F. D. Marques, E. M. Belo, V. A. Oliveira, J. R. Rosolen, and A. R. Simoni, "Non-linear phenomena analysis of stall-induced aeroelastic oscillations," in *Proceedings of the 45th AIAA/ASME/ASCE/AHS/ASC Structures, Structural Dynamics and Materials Conference*, vol. 6, pp. 4507–4513, Palm Springs, Calif, USA, April 2004.

[31] A. R. Simoni, *Análise de séries temporais esperimentais não lineares*, Ph.D. thesis, Escola de Engenharia de São Carlos, Universidade de São Paulo, São Paulo, Brazil, 2007.

[32] A. Wolf, J. B. Swift, H. L. Swinney, and J. A. Vastano, "Determining Lyapunov exponents from a time series," *Physica D*, vol. 16, no. 3, pp. 285–317, 1985.

[33] F. D. Marques, R. M. G. Vasconcellos, and A. R. Simoni, "Analysis of an experimental aeroelastic system through nonlinear time series," in *Proceedings of the International Symposium on Dynamic Problems of Mechanics (DINAME '09)*, Angra dos Reis, Brazil, March 2009.